Nanoscale

# First-principles study of the oxidation susceptibility of $WS_2$, $WSe_2$, and $WTe_2$ monolayers



| | |
|---|---|
| Journal: | *Nanoscale* |
| Manuscript ID | NR-ART-11-2023-006089.R1 |
| Article Type: | Paper |
| Date Submitted by the Author: | 03-Feb-2024 |
| Complete List of Authors: | Rawat, Ashima ; Michigan Technological University, Physics<br>Patra, Lokanath; University of California Santa Barbara, ;<br>Pandey, Ravi; Michigan Technological University, Department of Physics<br>Karna, Shashi; Army Research Laboratory, |
| | |

# First-principles study of the oxidation susceptibility of $WS_2$, $WSe_2$, and $WTe_2$ monolayers

Ashima Rawat[*1], Lokanath Patra[2], Ravindra Pandey[1] and Shashi P. Karna[*3]

[1]*Department of Physics, Michigan Technological University, Houghton, MI, 49931, USA*

[2]*Department of Mechanical Engineering, University of California, Santa Barbara, Santa Barbara, CA 93106-5070, USA.*

[3]*DEVCOM Army Research Laboratory, Weapons, and Materials Research Directorate, ATTN: FCDD-RLW, Aberdeen Proving Ground, Aberdeen, Maryland 21005-5069, USA*

(Feb 1, 2024)

Corresponding Authors: arawat2@mtu.edu, shashi.p.karna.civ@army.mil

## Abstract

The environmental stability of two-dimensional (2D) transition-metal dichalcogenide monolayers is of great importance for their applications in electronic, photonic, and energy-storage devices. In this study, we focus on understanding the susceptibility of $WS_2$, $WSe_2$, and $WTe_2$ monolayers to oxygen exposure in the form of atomic oxygen, $O_2$, and $O_3$ molecules, respectively. Calculations based on the van der Waals corrected density functional theory predict $O_2$ and $O_3$ molecules to be weakly adsorbed on these monolayers, though atomic oxygen prefers chemisorption accompanied by a significant charge transfer from the surface to oxygen. In the physisorbed molecular configurations consisting of $O_2$, and $O_3$, the partially oxidized monolayers retain their geometrical and electronic structures. The calculated transition path as the oxygen approaches the surface shows a high-energy barrier for all cases, thus explaining the photo-induced formation of the oxidized configurations in the experiments. Furthermore, oxidizing the $WS_2$ monolayer is predicted to modify its electronic structure, reducing the bandgap with increasing oxygen coverage on the surface. Overall, the calculated results predict the resilience of $WS_2$, $WSe_2$, and $WTe_2$ monolayers against oxygen exposure, thus ensuring stability for devices fabricated with these monolayers.

## 1 Introduction

Two-dimensional (2D) semiconductors, especially transition metal dichalcogenides (TMDs), such as $WX_2$ and $MoX_2$ (X: S, Se, Te) have emerged as an attractive class of materials for a wide range of applications in electronics and optoelectronics devices because of their unique electronic properties, such as high carrier mobility, tunable band gap, and anisotropic electron transport.[1-11] However, their device applications also encounter challenges due to their enhanced susceptibility to oxidation in ambient conditions. This, rather undesirable chemical property has drawn considerable attention in understanding the stability and oxidation behavior of TMDCs, especially $WS_2$ and $MoS_2$.[12-15] In a recent study of thermal stability, Rahman et al[16] found that the monolayer $MoS_2$ is quite stable up to a temperature of 1300 K against oxidation. However, at 1400 K, oxidation initiation begins, and by 1500 K, $MoS_2$ readily reacts with $O_2$. Another study by Zhao et al. delved into $O_2$ adsorption on both pristine and defective TMD monolayers. The research highlighted the inert nature of defect-free TMDs to $O_2$, while oxidation, an exothermic process, primarily occurred at chalcogen vacancies with adsorption energies ranging from 1.8 to 3.9 eV.[17] Investigations on bilayer $MoS_2$ demonstrated a substantial reduction in the "ON" state current under ambient conditions. The reduced current was attributed to additional scattering centers from chemisorption on defect sites, indicating the sensitivity of TMDs to ambient conditions and the impact on electronic properties.[18] For the case of $WS_2$, a recent experimental study has demonstrated its oxidation under exposure to UV light, but this photo-oxidation of $WS_2$ is not fully understood.[19] These studies collectively provide an enhanced understanding of the susceptibility of TMDs toward oxidation and its implications on device performance. However, this understanding also raises the question: (1) What is the mechanism of oxidation of TMDs? (2) What kind of oxidative species are more effective in oxidizing TMDs, thereby affecting the electronic band structure and other electronic properties? To address these questions, we have systematically studied the reaction of three oxidizing species, namely free O atom, and $O_2$ and $O_3$ molecules with $WS_2$, $WSe_2$, and $WTe_2$ within the framework of the density functional theory (DFT) and the climbing image nudged elastic band (CINEB) methods. Our emphasis will be on understanding the effects on geometrical and electronic structure and trying to develop a detailed understanding of the oxidation process in terms of chemical bonding, dissociation energy, and density of states in the current study.

## 2 Computational Method

DFT-based calculations using the projected augmented wave (PAW) pseudopotential[20] were performed as implemented in the Vienna ab initio simulation package (VASP).[21-24] The Perdew–Burke–Ernzerhof form of the generalized gradient approximation (PBE-GGA)[25] was used, along with the van der Waals (vdW) correction term (D3) proposed by Grimme.[26] The convergence criteria for energy and the Hellman Feynman force acting on each atom were set to $10^{-6}$ eV and 0.01 eV/Å, respectively. The Brillouin zone was sampled using a centered k-point grid of size (12×12×1). A (2×2×1) periodic supercell was constructed for the monolayers, and periodic image interactions were minimized by using a vacuum of 15 Å along the z-axis direction. The dynamical stability of the system was determined by calculating the phonon frequencies using the PHONOPY package [27,28], for which the force constants were obtained using the density functional perturbation theory.[29]

The oxygen adsorption energy ($E_{adsorption}$) was calculated using the following expression.[30-34]

$$E_{adsorption} = E_{(oxygen+WX2)} - (E_{(WX2)} + E_{(oxygen)}) \quad [1]$$

where $E_{(oxygen+WX2)}$ is the total energy of the adsorbed configuration, $E_{(WX2)}$ is the total energy of the pristine monolayer, and $E_{(oxygen)}$ is the total energy of an oxygen (atomic oxygen or $O_2$ or $O_3$ molecule).

The CINEB method,[35] as implemented in VASP, was employed to calculate the minimum energy paths describing the interaction between an oxygenous species, atomic oxygen, $O_2$, and $O_3$ molecule, respectively, and a TMD monolayer. The CINEB method generates a set of six intermediate configurations (i.e., images) from the predetermined initial and final configurations. The initial (non-interacting) configuration consists of a molecule about 4.5 Å above the surface for these calculations. The final configuration consists of dissociated oxygens (atomic oxygen or $O_2$ or $O_3$ molecule) adsorbed on the monolayer.[36]

## 3.0 Results and Discussion

Figure 1 shows the hexagonal (2x2) supercell considered for the calculations. For the pristine $WS_2$, $WSe_2$, and $WTe_2$ monolayers, the calculated lattice constants and bandgaps have been described in Table 1 and the band structures have been provided in Fig S1, Electronic Supplementary Information (ESI) which are in good agreement with the previously reported DFT values. Table S1 (ESI) lists the structural properties of $O_2$ and $O_3$ molecules calculated at the DFT (GGA) level of theory and are reasonably good agreement with reported theoretical and

experimental values ($O_2$: 1.24 Å (DFT)[41], 1.21 Å (experiment)[42] and $O_3$: 1.28 Å (DFT[43] and experiment[44]), 116.49° (experiment)[43] and 117.90°(DFT).[44]

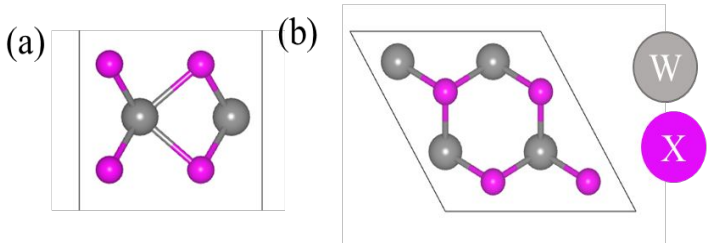


Figure 1. (a) Side (b) top views of the pristine $WS_2$, $WSe_2$, and $WTe_2$ monolayers. Color codes: gray: W, pink: chalcogen (S/Se/Te).

Table 1. Lattice Parameters and Bandgaps for $WX_2$ monolayers calculated at the PBE-DFT level of theory.

| Monolayers | a=b (Å) | Bandgap eV |
|---|---|---|
| $WS_2$ | 3.18 (3.18 [37,38]) | 1.86 (1.81[37,38]) |
| $WSe_2$ | 3.31 (3.31[37], 3.32[39,40]) | 1.57 (1.55[37], 1.53[40]) |
| $WTe_2$ | 3.56 (3.56 [37]) | 1.08 (1.02[37]) |

The equilibrium configurations of the oxygen adsorbed at $WS_2$, $WSe_2$, and $WTe_2$ monolayers are shown in Figure 2. Three different surface sites were considered for adsorption calculations: $(Chalcogen)_{top}$, $W_{top}$, and Hollow. Interestingly, the energetically preferred sites, shown in Figure 2, consist of an O forming a bond with the chalcogen atom (i.e., the $(Chalcogen)_{top}$ site). The remaining O atoms in $O_2$ and $O_3$ are slightly elongated parallel to the surface approaching the neighboring chalcogen atom. Table 2 lists the adsorption energy ($E_{adsorb}$), dissociation energy ($E_{diss}$), molecule-surface distance ($R_{X-O}$), charge transferred from the surface to molecule ($Q_o$), and activation barrier height ($E_{barrier}$) describing the interaction of O, $O_2$, and $O_3$ with the $WS_2$, $WSe_2$, and $WTe_2$ monolayers. Note that the dissociation energy ($E_{diss}$) is calculated as the difference between the total energy of the dissociated configuration (i.e., $O_2$ -> O+O or $O_3$ -> O+O+O) and the non-interacting configuration consisting of a molecule about 4.5 Å above the surface.[36]

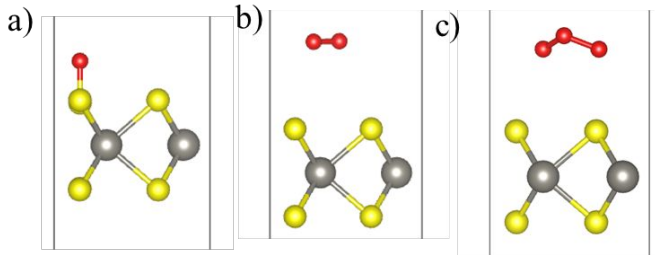


Figure 2. The calculated equilibrium configurations O, $O_2$, and $O_3$ molecules adsorbed on $WS_2$ monolayer. Color code: S (yellow), W (gray), and O (red).

Atomic oxygen interacting with the $WS_2$, $WSe_2$, and $WTe_2$ monolayers tends to chemisorb itself onto the top of the chalcogen atom (i.e., S or Se or Te) with an equilibrium bond distance, $R_{x-o}$, of 1.48, 1.65, and 1.85 Å for $WS_2$, $WSe_2$, and $WTe_2$, respectively. The calculated $E_{adsorb}$ is - 3.92, -3.0, and -3.44 eV for $WS_2$, $WSe_2$, and $WTe_2$, respectively. We note that atomic oxygen forms an ionic-covalent bond with an S atom of $WS_2$ as in the SO molecule for which $R_{S-O}$ is 1.48 Å.[45] The bonding follows a relatively large charge transfer (1.91e) from the monolayer (S) to atomic O, thereby resulting in chemisorption on the surface. A lesser degree of ionicity is predicted for the Se-O and Te-O bonds for the chemisorbed complexes on $WSe_2$ and $WTe_2$ monolayers. In the context of monolayers composed of $WX_2$, the interaction between tungsten (W) and chalcogen (X) atoms is characterized by a reduction in the charge transfer from W to X, i.e. $\Delta Q$ = 1.31e, 0.56 e, 0.11 e for $WS_2$, $WSe_2$, and $WTe_2$ respectively.[46] Hence the affinity of oxygen making bond with S is much higher than the Se and Te since S has more charge than the Se/Te. Furthermore, an inspection of the partial density of states (Fig. S2, ESI) shows that chemisorption of atomic oxygen does not induce gap states in the bandgap of the $WS_2$, $WSe_2$, and $WTe_2$ monolayers.

In contrast to the atomic oxygen chalcogenide interaction, the $O_2$ and $O_3$ molecules prefer a weakly physisorbed configuration on top of the $WS_2$, $WSe_2$, and $WTe_2$ monolayers with much lower $E_{adsorb}$ in the range of 0.03-0.16 eV with corresponding bond distance, $R_{x-o}$, of about ≈ 3 Å or greater in their equilibrium configurations (Table 2).

This contrasting nature of adsorption can be attributed to strong O-O bond (s) with bond dissociation energies of 5.11 and 6.27 eV in $O_2$ and $O_3$ molecules, respectively, [47] which prohibits a strong interaction with surface chalcogen atoms of the $WS_2$, $WSe_2$, and $WTe_2$ monolayers. To assess the feasibility of charge transfer from the surface to the molecules, we have compared the relative positions of the Fermi levels of the monolayers with the lowest unoccupied molecular

levels (LUMO) of the $O/O_2/O_3$ molecules.[36,48] From Figure 3 we note that for $WSe_2$ and $WTe_2$ monolayers, the Fermi levels lie above the O, $O_2$, and $O_3$ levels, whereas for $WS_2$ the Fermi level straddle only the O and $O_3$ levels. We can, thus, expect finite charge transfer in all the adsorption cases except for the $O_2$ on the $WS_2$ monolayer. We quantified this charge transfer using Bader charge analysis presented in Table 2 which confirms that there is almost no charge transfer in the case of $O_2$ physisorbed on $WS_2$ monolayer as displayed in Figure 3. It is worth noting that, in the weakly physisorbed configurations both $O_2$ and $O_3$ retain their structural identity in terms of the bond length and bond angles: R(O-O) is 1.24 Å for the $O_2$ complexes, and (R(O-O), A(O-O-O) are (1.29 Å, 117.5°), (1.30 Å, 117.0°), and (1.31 Å, 116.3°) for the $O_3$-$WS_2$, $O_3$-$WSe_2$, and $O_3$-$WTe_2$ complexes, respectively. The calculated value R(O-O) for isolated $O_2$ and $O_3$ molecules is 1.24 Å and 1.28 Å, respectively. Note that the adsorption energy of the $O_2$ molecule for the pristine $MoS_2$ was reported to be 58 meV.[49]

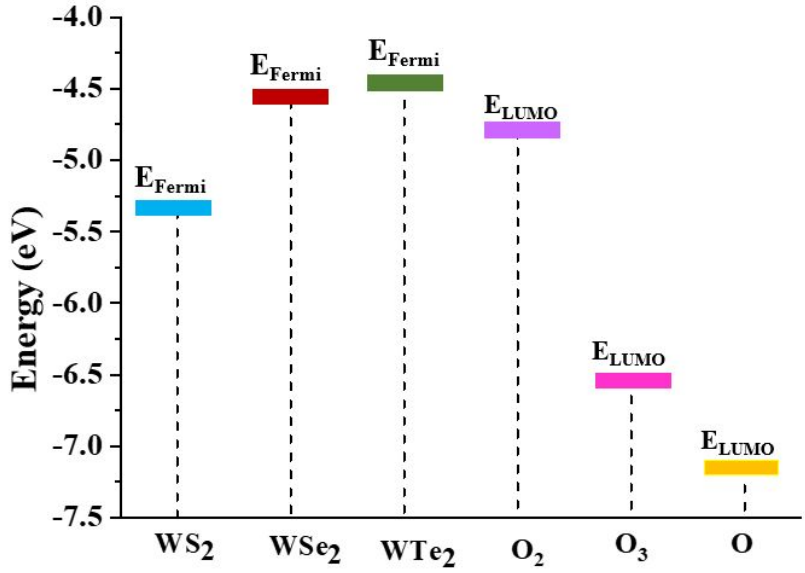


Figure 3. A schematic diagram displaying the monolayer's Fermi level ($E_{Fermi}$) and the lowest unoccupied molecular orbital ($E_{LUMO}$) of the atomic O and molecular $O_2$ and $O_3$.

Table 2. $WS_2$, $WSe_2$, and $WTe_2$ monolayers interacting with O, $O_2$, and $O_3$: the calculated adsorption energy per oxygen atom ($E_{adsorb}$), dissociation energy ($E_{diss}$), molecule-surface distance ($R_{X-O}$), charge transferred from the surface to molecule ($Q_o$), and the energy barrier height for dissociation ($E_{barrier}$).

| | Monolayer | | $WS_2$ | $WSe_2$ | $WTe_2$ |
|---|---|---|---|---|---|
| O | Chemisorption | $E_{adsorb}$, eV/atom | -3.92 | -3.00 | -3.44 |
| | | $R_{x-o}$, Å | 1.48 | 1.65 | 1.85 |
| | | $Q_0$ /O atom | 1.91 e | 0.86 e | 0.98 e |
| $O_2$ | Physisorption | $E_{adsorb}$, eV/atom | -0.05 | -0.03 | -0.16 |
| | | $R_{x-o}$, Å | 3.39 | 3.59 | 3.67 |
| | | $Q_0$ /O atom | ≈0.0 e | 0.03 e | 0.08 e |
| | Dissociation | $E_{diss}$, eV | -0.96 | 1.23 | 0.28 |
| | | $R_{x-o}$, Å | 1.48 | 1.65 | 1.82 |
| | | $Q_0$/O atom | 1.9 e | 0.81 e | 1.08 e |
| | | $E_{barrier}$, eV | 5.47 | 5.17 | 5.05 |
| $O_3$ | Physisorption | $E_{adsorb}$, eV/atom | -0.07 | -0.08 | -0.14 |
| | | $R_{x-o}$, Å | 3.05 | 2.95 | 2.93 |
| | | $Q_0$/O atom | 0.06 e | 0.15 e | 0.22 e |
| | Dissociation | $E_{diss}$, eV | -1.43 | 1.04 | ≈0 |
| | | $R_{x-o}$ (Å) | 1.48 | 1.65 | 1.82 |
| | | $Q_0$ /O atom | 1.88 e | 0.58 e | 0.77 e |
| | | $E_{barrier}$, eV | 6.03 | 7.30 | 6.85 |

Next, we calculate the transition path taken by both $O_2$ and $O_3$ molecules approaching the surface using the CINEB method, as displayed in Figure 4. Here, the initial (non-interacting) configuration consisted of a molecule placed at ~ 4.5 Å above the monolayer, and the final configuration consisted of the dissociated atomic oxygen forming the bonds with the surface atoms (i.e., S or Se or Te) of the monolayers.

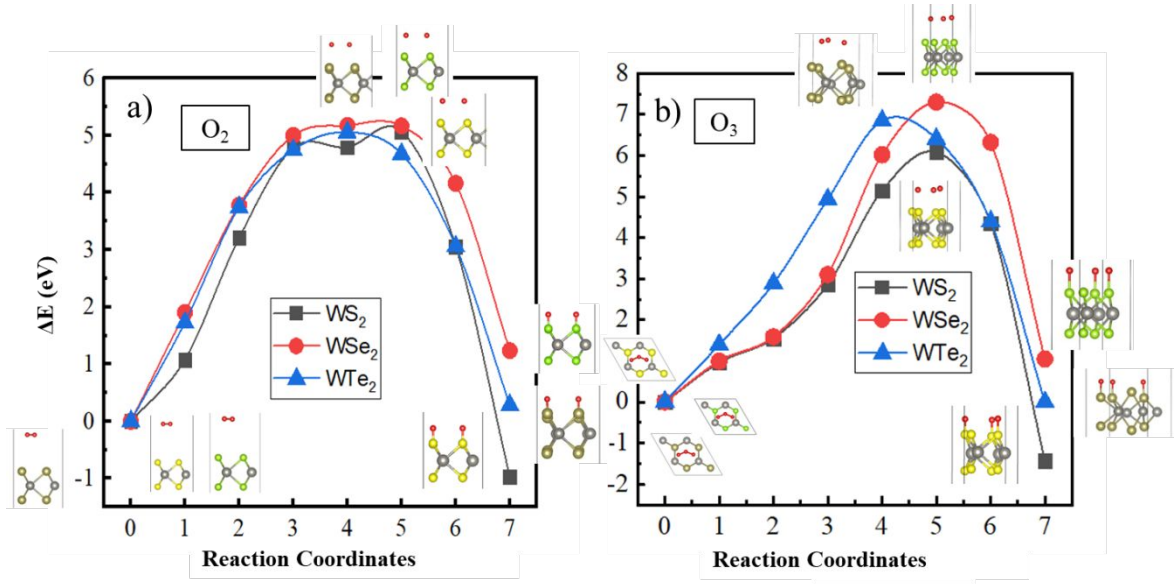


Figure 4. The molecular transition path on $WS_2$, $WSe_2$, and $WTe_2$ monolayers for (a) $O_2$ and (b) $O_3$ molecules were calculated using the CINEB method.

The calculated molecular transition path exhibits a relatively high-energy barrier for either $O_2$ or $O_3$ dissociation on these monolayers. The energy barrier for the $O_2$ dissociation to atomic oxygens is calculated to be ≈ 5 eV, whereas that for the $O_3$ dissociation to atomic oxygens is predicted to be ≥ 6 eV (Table 2). Notably, among the investigated monolayers, only the $WS_2$ monolayer preferred the oxidized configurations with an $E_{dissociation}$ of ≈ -0.96 eV for $O_2$ and -1.43 eV for $O_3$ relative to the non-interacting configurations. This can be attributed to the ease with which S-O bonds can form on the $WS_2$ monolayer relative to Se-O or Te-O surface bonds for the other monolayers. The oxidized $WSe_2$ or $WTe_2$ monolayers are not predicted to be energetically preferred (Table 2). It should be noted that experiments have been performed on the diatomic molecules SO, SeO, and TeO, reporting their vibrational properties.[50]

After recognizing that a partially oxidized $WS_2$ monolayer (with 25% surface coverage), can be stable, we now examine the electronic properties and the stability of the fully oxidized $WS_2$ monolayer, (with 100% surface coverage).

In the equilibrium configuration of the oxidized $WS_2$ monolayer, the calculated S-O bond length is 1.48 Å, similar to that predicted for a partially oxidized $WS_2$ surface (Table 2). Another striking feature appears in the calculated total density of states at the Fermi level for the oxidized $WS_2$ monolayer, as shown in Figure 5. On comparing the pristine $WS_2$ (Figure 5a) to the partially oxidized one (Figure 5b), we observe that the bandgap reduces by 0.36 eV, and as we move away from the Fermi level in the valence states, new hybridized S-O states appear due to the formation of

S-O bonds. A similar observation has been made for SnS/SnSe/GeS/GeSe monolayers where oxygen chemisorption leads to bandgap reduction with the activation barrier $O_2$ in the range from 1.26 to 1.60 eV.[51] Notably, these studies did not address the oxidation of the monolayers by atomic O, and $O_3$ molecule.

Further comparison with the fully oxidized, (Figure 5a) monolayer, the band gap reduces from 1.86 eV (pristine) to 1.50 eV (Figure 5b) for partially oxidized to 0.30 eV for the fully oxidized $WS_2$ monolayer and the hybridized states appear near the Fermi level due to the increase in the S-O bonds. In the case of a partially oxidized $WS_2$ monolayer (Figure 5b), the upper valence band (width of 6 eV) consists of the dominating S-O bonds with small contributions from W-O bonds. In the fully oxidized monolayer, however, the upper valence band splits into two parts; the S-O band has moved down to about 4 eV relative to the Fermi level as can be seen from Figure 5c. The reduction in the bandgap in TMDs with oxidation has also been previously reported by DFT calculations.[52]

To assess the dynamic stability of the fully oxidized $WS_2$, the phonon dispersion calculations were performed using the PHONOPY package. Figure 6b displays the calculated phonon dispersion relationship, in which a small pocket of negative frequencies (<0.25 THz) near Γ along Γ-M direction in the Brillouin zone is noticed. We believe this small pocket of negative frequencies is an artifact of the technical details such as supercell size and functional used[53] in the present study. Otherwise, the calculated phonon band structure for the pristine $WS_2$ monolayer (displayed in Figure 6a) is in good accord with the earlier published reports.[54] A comparison of the phonon band structures of the oxidized $WS_2$ monolayer with the pristine one, clearly shows a distinct phonon branch appearing at approximately 33 THz, which typically corresponds to the S-O bond stretching frequency.[55]

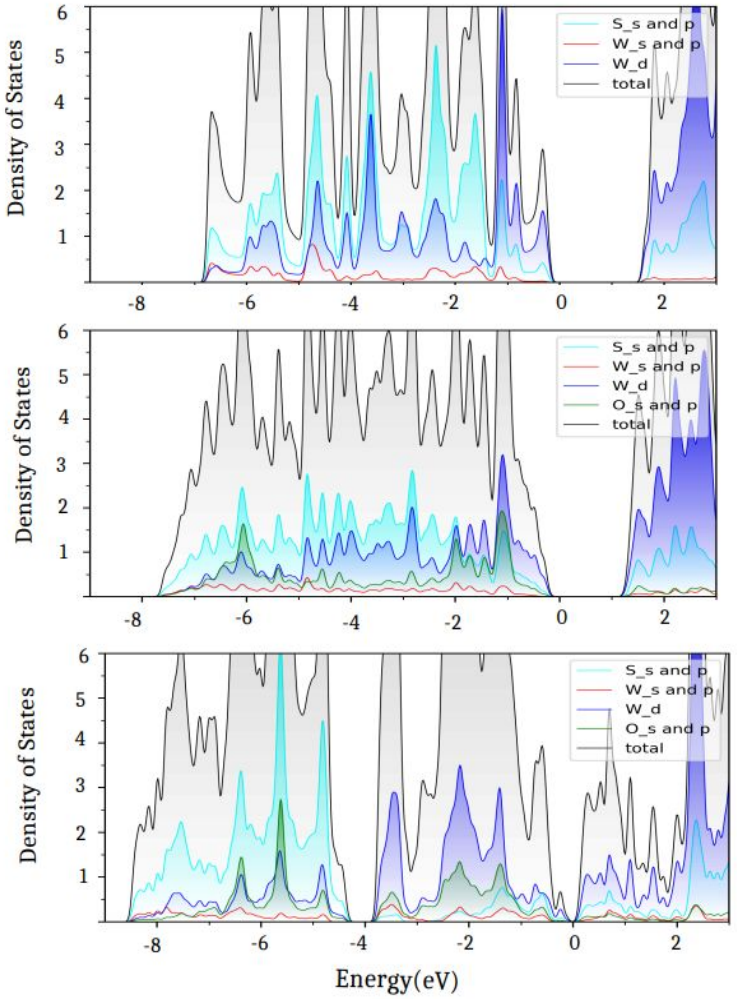


Figure 5. Projected Density of states for (a) pristine, (b) partially oxidized, and (c) fully oxidized $WS_2$ monolayer.

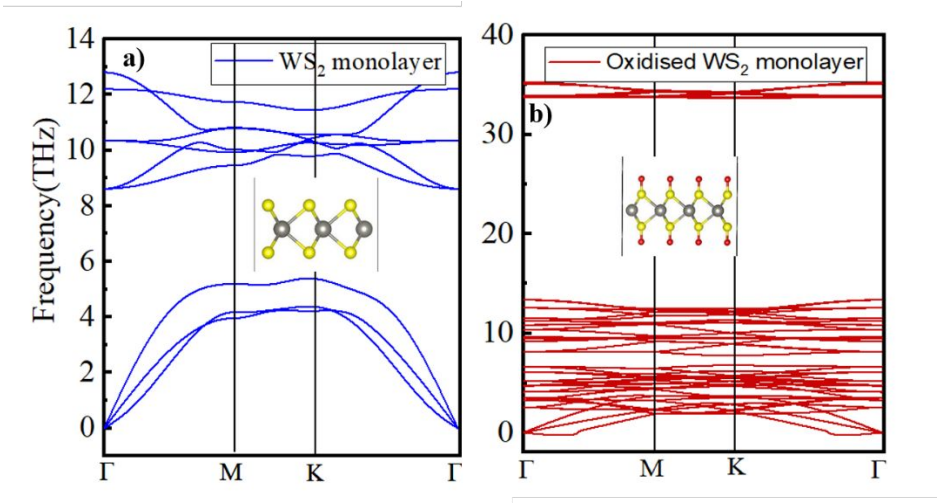


Figure 6. The calculated phonon dispersion curves for (a) pristine and (b) oxidized $WS_2$, monolayer.

## 4.0 Summary

The oxidation susceptibility/resistance of $WS_2$, $WSe_2$, and $WTe_2$ monolayers was investigated from their interaction with atomic oxygen, $O_2$, and $O_3$ molecules, respectively. Calculations using van der Waals corrected density functional theory (DFT) predict the strongly chemisorbed O in the case of interaction with atomic oxygen, but weakly physisorbed $O_2$ and $O_3$ on the monolayer surface. These results are in accordance with a significant charge transfer from surface to atomic oxygen for all the cases. The weakly physisorbed $O_2$ and $O_3$ molecules retain their molecular configurations at about 3.0 Å or more above the surface. The CINEB calculations predict a large energy barrier for either $O_2$ or $O_3$ to dissociate into atomic oxygens on the surface. Interestingly, the oxidized $WS_2$ is energetically preferred over the pristine $WS_2$, though the energy barrier is about 5.5 eV, which explains the experimental observation of high resistance of $WS_2$ to ambient oxidation for up to ten months but is susceptible to photo-induced oxidation.

## Acknowledgment

The authors would like to thank the computational facilities provided by Michigan Technological University. The Funding from the Army Research Office through grant no. W911NF-14-2-0088 for partial support of this research at the Michigan Tech University (RP) is gratefully acknowledged.

## References


1. M. Chhowalla, H. S. Shin, G. Eda, L. J. Li, K. P. Loh, H. Zhang, *Nat. Chem.*, 2013, **5**, 263-275.
2. Y. Guo, C. Liu, Q. Yin, C. Wei, S. Lin, T. B. Hoffman, Y. Zhao, J. H. Edgar, Q. Chen, S. P. Lau, J. Dai, H. Yao, H.-S. P. Wong, Y. Chai, *ACS Nano*, 2016, **10**, 8980-8988.
3. G. R. Bhimanapati, Z. Lin, V. Meunier, Y. Jung, J. Cha, S. Das, D. Xiao, Y. Son, M. S. Strano, V. R. Cooper, *ACS Nano*, 2015, **9**, 11509-11539.
4. Z. Wang, B. Mi, *Environ. Sci. Technol.*, 2017, **51**, 8229-8244.
5. E. Singh, K. S. Kim, G. Y. Yeom, H. S. Nalwa, *ACS Appl. Mater. Interfaces*, 2017, **9**, 3223-3245.
6. Y. Wu, N. Joshi, S. Zhao, H. Long, L. Zhou, G. Ma, B. Peng, O. N. Oliveira Jr., A. Zettl, L. Lin, *Appl. Surf. Sci.*, 2020, **529**, 147110.
7. X. Chen, C. Liu, S. Mao, *Nano-Micro Lett.*, 2020, **12**, 1-24.
8. S. Kuriakose, T. Ahmed, S. Balendhran, V. Bansal, S. Sriram, M. Bhaskaran, S. Walia, *2D Mater.*, 2018, **5**, 032001.
9. Q. H. Wang, K. Kalantar-Zadeh, A. Kis, J. N. Coleman, and M. S. Strano. *Nat. Nanotechnol.* 2012, **7**, 699-712
10. B. Radisavljevic, A. Radenovic, J. Brivio, V. Giacometti & A. Kis, *Nat. Nanotech.*, 2011, **6**, 147–150.
11. X.-L. Fan, Y. Yang, P. Xiao, W.-M. Lau, *J. Mater. Chem. A*, 2014, **2**, 20545-20551.
12. Joshua O Island, Gary A Steele, Herre S J van der Zant, and Andres Castellanos-Gomez. 2D Materials, 2015, **2**, 011002.
13. Gaoxue Wang, William J Slough, Ravindra Pandey, and Shashi P Karna, 2D Materials, 2016, **3**, 025011.
14. Q. Zhao, R. Frisenda, P. Gant, D. Perez de Lara, C. Munuera, M. Garcia-Hernandez, Y. Niu, T. Wang, W. Jie, A. Castellanos-Gomez, Adv. Funct. Mater., 2018, **28**, 1805304.
15. B. Chamlagain, S. I. Khondaker, ACS Omega, 2021, **6**, 24075-24081
16. Md H. Rahman, Emdadul H. Chowdhury, Sungwook Hong, *Surfaces and Interfaces*, 2021, 26, 101371.
17. H. Liu, N. Han, J. Zhao, *RSC Adv.*, 2015, **5**, 17572-17581.
18. H. Qiu, L. Pan, Z. Yao, J. Li, Y. Shi, X. Wang, *Appl. Phys. Lett.*, 2012, **100**, 123104.
19. J. C. Kotsakidis, Q. Zhang, A. L. Vazquez de Parga, M. Currie, K. Helmerson, D. K. Gaskill, M. S. Fuhrer, *Nano Lett.*, 2019, **19**, 5205-5215.
20. P. E. Blöchl, *Phys. Rev. B*, 1994, **50**, 17953.
21. G. Kresse, J. Furthmüller, *Phys. Rev. B*, 1996, **54**, 11169.
22. G. Kresse, J. Hafner, *Phys. Rev. B*, 1993, **47**, 558.
23. G. Kresse, J. Hafner, *Phys. Rev. B*, 1994, **49**, 14251.
24. G. Kresse, J. Furthmüller, *Comput. Mater. Sci.*, 1996, **6**, 15-50.
25. J. P. Perdew, K. Burke, M. Ernzerhof, *Phys. Rev. Lett.*, 1996, **77**, 3865.
26. S. Grimme, S. Ehrlich, L. Goerigk, *J Comput. Chem.*, 2011, **32**, 1456-1465.
27. A. Togo, F. Oba, I. Tanaka, *Phys. Rev. B*, 2008, **78**, 134106.
28. A. Togo, I. Tanaka, *Scripta Materialia*, 2015, **108**, 1-5.
29. S. Baroni, S. De Gironcoli, A. Dal Corso, P. Giannozzi, *Rev. Mod. Phys.*, 2001, **73**, 515.
30. A. Zaman, R. Shahriar, S. T. Hossain, M. R. Akhond, H. T. Mumu, A. Sharif, *RSC Adv.*, 2023, **13**, 23558-23569.
31. M. A. Islam, H. Li, S. Moon, S. S. Han, H.-S. Chung, J. Ma, C. Yoo, T. J. Ko, K. H. Oh, Y. Jung, Y. Jung, *ACS Appl. Mater. Interfaces*, 2020, **12**, 53174–5318
32. T. Liu, Y. Chen, M. Zhang, L. Yuan, C. Zhang, J. Wang, J. Fan, AIP Advances, 2017, **7**, 125007.
33. D. Bahamon, M. Khalil, A. Belabbes, Y. Alwahedi, L. F. Vega, K. Polychronopoulou, *RSC Adv.*, 2021, **11**, 2947-2957.
34. H. Wei, Y. Gui, J. Kang, W. Wang, C. Tang, *Nanomaterials*, 2018, **8**, 646.
35. G. Henkelman, B. P. Uberuaga, and H. Jónsson, J. Chem. Phys, 2000, **113**, 9901-9904.
36. L. Patra, G. Mallick, R. Pandey, and S. P. Karna, Appl. Surf. Sci., 2022, **588**, 152940.
37. A. Rawat, N. Jena, and A. De Sarkar, J. Mater. Chem. A, 2018, **6**, 8693-8704.

38. Y. Ma, Y. Dai, M. Guo, C. Niu, J. Lu, and B. Huang, Phys. Chem. Chem. Phys, 2011, **13**, 15546-15553.
39. D. Le, A. Barinov, E. Preciado, M. Isarraraz, I. Tanabe, T. Komesu, C. Troha, L. Bartels, T. S. Rahman, P. A. Dowben, *J. Phys.: Condens. Matter*, 2015, **27**, 182201.
40. P. Manchanda and R. Skomski, J. Phys. Condens. Matter, 2016, **28**, 064002.
41. A. Panchenko, M. T. M. Koper, T. E. Shubina, S. J. Mitchell, E. Roduner, J. Electrochem. Soc., 2004, **151**, A2016-A2027.
42. H. Nakatsuji and H. Nakai, Chem. Phys. Lett., 1992, **197**, 339.
43. R. Trambarulo, S. N. Ghosh, C. A. Burrus Jr, W. Gordy, *J. Chem. Phys.*, **1953**, 21, 851-855
44. Davood Farmanzadeh, Nastaran Askari Ardehjani, Appl. Surf. Sci., 2018, **444**, 642-649.
45. N. N. Greenwood and A. Earnshaw, Chemistry of the Elements, Elsevier, 2012.
46. Li, N. V. Medhekar, V. B. Shenoy, *J. Phys. Chem. C*, **2013**, 117, 15842-15848
47. B. W. Pfennig, Principles of Inorganic Chemistry, John Wiley & Sons, 2021
48. IBM Journal of Research and Development, 1960, **4**, 283-287.
49. H. Liu, N. Han, and J. Zhao, RSC Adv., 2015, **5**, 17572-1758.
50. P. Haranath, P. T. Rao, and V. Sivaramamurty, Zeitschrift für Physik A Hadrons and Nuclei, 1959, **155**, 507-517.
51. Y. Guo, S. Zhou, Y. Bai, J. Zhao, ACS Appl. Mater. Interfaces, 2017, **9**, 12013-12020.
52. K. Iordanidou, M. Houssa, G. Pourtois, V. V. Afanas'ev, and A. Stesmans, Phys. Status Solidi RRL, 2016, **11**, 787–791.
53. V. Zólyomi, N. D. Drummond, and V. I. Fal'ko, Phys. Rev. B, 2014, **89**, 205416.
54. A. Berkdemir, H. R. Gutiérrez, A. R. Botello-Méndez, N. Perea-López, A. L. Elías, C.-I. Chia, B. Wang, V. H. Crespi, F. López-Urías, J.-C. Charlier, H. Terrones, and M. Terrones, *Sci. Rep.*, 2013, **3**, 1755.
55. K. I. Oh and C. R. Baiz, J. Chem. Phys, 2019, 151, **23**, 234107.